Supporting Information

Resolution Enhancement in Solid-State NMR of Oriented Membrane Proteins by Anisotropic Differential Linebroadening

Thomas Vosegaard,[¶,*] Kresten Bertelsen,[¶] Jan M. Pedersen,[¶] Lea Thøgersen,[¶] Birgit Schiøtt,[¶] Emad Tajkhorshid,[§] Troels Skrydstrup,[¶] and Niels Chr. Nielsen[¶]

[¶]*Center for Insoluble Protein Structures (inSPIN), Interdisciplinary Nanoscience Center (iNANO) and Department of Chemistry, University of Aarhus, Langelandsgade 140, DK-8000 Aarhus C, Denmark.* [§]*Department of Biochemistry and Beckman Institute, University of Illinois at Urbana-Champaign, 405N, Mathews, Urbana, IL 61801, USA.*

E-mail: tv@chem.au.dk

1. Preparation of ^{15}N-Aib$_8$ alamethicin in oriented DMPC bilayers

Synthesis of N-Fmoc-^{15}N-Aib

The amino acid Aib (^{15}N-2-Amino-2-methyl propionic acid/α-amino isobutyric acid) was synthesized as previously described (S1). Addition of the Fmoc protection group was performed as recently described for Fmoc-Aib-d$_6$ (S2), and afforded *N*-Fmoc-^{15}N-Aib (2.98 g, 68%) as a colorless solid. We note that since this synthesis starts from very cheap materials, even in the case of synthesis with ^{15}N labeling, the cost of labeling this amino acid remains significantly cheaper than the price of commercially available ^{15}N labeled Fmoc amino acids. ^{1}H NMR (400 MHz, CD_3OD) δ (ppm) 12.31 (s, 1H, CO_2H), 7.75 (d, 2H, J = 7.6 Hz), 7.65 (d, J = 7.2 Hz, 2H), 7.38-7.34 (m, 2H), 7.29 (dt, J = 7.2, 1.2 Hz, 2H), 4.29 (m, 2H), 4.18 (t, J = 7.0 Hz, 1H), 1.48 (s, 6H). ^{13}C NMR (100 MHz, CD_3OD) δ (ppm) 178.3, 157.5, 145.3 (2C), 142.5 (2C), 128.7 (2C), 128.1 (2C), 126.2 (2C), 120.9 (2C), 67.6, 57.1, 57.0, 25.6 (2C). HRMS (ES-TOF) $C_{19}H_{19}{}^{15}NO_4$ [M+Na$^+$]: 349.1290. Found: 349.1289.

Synthesis of ^{15}N-Aib$_8$-alamethicin

The sequence of alamethicin employed in this work corresponds to alamethicin F30/3: Ac-UPUAUAQU*VUGLUPVUUEQ-Phol, where the amino acids are listed in one-letter code with the following additional abbreviations: Acetyl (Ac), Aib (U), ^{15}N-Aib (U*), and *L*-phenylalaninol (Phol). The peptide was synthesized, cleaved from the resin, and purified as recently described for the deuterated variant (S2). The purity was confirmed by analytical HPLC to be >90%. MS (MALDI-TOF) $C_{92}H_{150}{}^{15}N_1N_{21}O_{25}$ [M+Na$^+$]: 1987.1. Found 1987.1.

Preparation of ^{15}N-Aib$_8$-alamethicin in oriented lipid bilayers

Dry 1,2-Dimyristoyl-*sn*-Glycero-3-Phosphocholine (DMPC) was achieved from a commercial DMPC solution in chloroform (Avanti polar lipids, Alabaster, AL) by overnight evaporation under vacuum. 5 mg lyophilized ^{15}N-Aib$_8$ alamethicin was dissolved in 384 μL methanol, and 25.4 mg dry DMPC was added. The solution was vortexed thoroughly to ensure complete dissolution of the lipids and peptide. Sixteen glass slides (7mm x 14mm x 0.05mm, SCHOTT Scandinavia A/S) were rinsed in a sonicator. The rinsing was done in three steps (20 min each), first in water, then in acetone, and finally in water. After the last rinsing the glass slides were dried in an oven at 40°C for 1 hour.

The lipid/peptide solution was distributed by two times 12 μL on each glass slide, and they were left at ambient temperature for 6 hours to allow evaporation of the organic solvent. To ensure complete removal of the solvent the slides were placed in vacuum overnight. The slides were then stacked and placed in a desiccator with 100% humidity at 37°C for 48 hours. Finally, the slides were gently squished, wrapped in parafilm, and sealed in a small plastic bag containing a piece of moistened cotton cloth.

2. Solid-state NMR experiments

All ^{15}N NMR experiments were performed on a 16.45-T (700 MHz) Bruker Avance-2 spectrometer with a ^{15}N Larmor frequency of 70.95 MHz using a Bruker triple-resonance flatcoil Bruker probe running in ^{1}H-^{15}N double-resonance mode. The 1D experiments were recorded using a standard CP experiment with a 4.5 μs ^{1}H 90° excitation pulse (56 kHz) followed by a 2 ms CP period with an ^{15}N rf field strength of 35 kHz and a ^{1}H rf field strength varying as a 20% ramp (from ~28 kHz to ~42 kHz). For the heteronuclear decoupling experiment SPINAL-64 decoupling (S3) with a ^{1}H rf field strength of 65 kHz and the carrier frequency at 10 ppm was used during 5 ms acquisition period. The experiment employed 4096 scans. For the FSLG-decoupled experiment the ^{1}H carrier offsets were changing between 10 ppm plus and minus 46 kHz for periods of 12.5 μs and with 180° phase shift to fulfill the FSLG condition with repeated $2\pi\overline{2\pi}$ pulses (with effective fields of 80 kHz) at the magic angle. This experiment employed 8192 scans. For the 2D separated-local-field (SLF) experiment the PISEMA (S4) pulse sequence was used. Following x-phase cross-polarization (CP) a $-y$-phase 35.3° (90° - θ_{MA}) pulse was applied on the ^{1}H channel, to allow spin locking along the magic angle, while retaining the spin lock of ^{15}N. The x-phase SEMA block employed ^{15}N and ^{1}H rf field strengths of 50 kHz and 40.8 kHz, and corresponding ± 28.9 kHz offsets on ^{1}H to simultaneously match the Hartmann-Hahn and FSLG conditions. This experiment employed 1024 scans for each of the 24 t_1 increments of 40 μs corresponding to an indirect spectral width of 25 kHz, which was increased to 30.62 kHz during the data treatment to compensate for the dipolar scaling factor of $\sqrt{3/2}$ during the SEMA block. All experiments employed a direct spectral width of 100 kHz, 3 s repetition delay, the ^{15}N carrier

frequency at 200 ppm, and a temperature of 30 ºC. The ^{15}N chemical shifts were referenced to an external sample of solid $^{15}NH_4Cl$ at 39.8 ppm.

3. Solid-state NMR simulations

Simulations of the oriented solid-state NMR experiments were performed using SIMPSON (S5,6) and SIMMOL (S6,7), and apart from the inclusion of mosaic spread, the theory is similar to that outlined our recent work on deuterated alamethicin (S2). Under the present experimental conditions, the alamethicin peptides will undergo fast rotational diffusion in the bilayer (S2,8,9). The fast rotation leads to an averaging of the nuclear spin interactions around the bilayer normal. The averaged nuclear spin interaction (λ) is axially symmetric and aligned with its unique axis along the bilayer normal, and has a reduced anisotropic value of

$$\lambda_{\mathrm{aniso}}^{\mathrm{reduced}} = \lambda_{\mathrm{aniso}} \kappa(\eta_\lambda, \Omega_{\mathrm{PE}}, \Omega_{\mathrm{EB}}). \qquad \text{(S1)}$$

Here, the anisotropy of the nuclear spin interaction is characterized by the magnitude (λ_{aniso}), asymmetry parameter (η_λ), and orientation relative to the lipid bilayer. In the present work we only consider the heteronuclear ^{1}H-^{15}N dipole-dipole coupling (b) and the ^{15}N chemical shift (δ), which are characterized by the anisotropic nuclear spin interaction parameters (b_{aniso}, η_{b}) = (9.94 kHz, 0) as determined from a model system (S10), and (δ_{aniso}, η_δ) = (104 ppm, 0.14) as determined from a lyophilized sample of ^{15}N-Aib$_8$ alamethicin prior to reconstituting it into lipid bilayers. For the chemical shift interaction, we further measured the isotropic shift to a value of δ_{iso} = 126 ppm. The orientation of the nuclear spin interaction tensors is obtained using a series of coordinate transformations starting at the principal axis frame (P) using the peptide-plane frame (E) and bilayer frame (B) as intermediate steps to the laboratory frame (L). Typical Euler angles for the peptide P ↔ E coordinate transformation (Ω_{PE}) are known from numerous studies (see ref. (S7) for details) and assume values of $\Omega_{\mathrm{PE}}(b)$ = (90°, 0°, 0°) and $\Omega_{\mathrm{PE}}(\delta)$ = (90°, 17°, 90°). The Euler angles relating the peptide frame to the bilayer frame are calculated based on the molecular geometry (here assuming ideal α-helical torsion angles ϕ,ψ = -65º, -40º) and helix tilt (τ) and rotational pitch (ρ) using SIMMOL as described elsewhere (S2,6,7,11,12). The geometric scaling factor (κ) in Eq. (S1) is obtained by the above series of coordinate-system transformations, and by averaging over the Euler angle γ_{EB} to account for the fast rotation around the bilayer normal:

$$\kappa(\eta_\lambda,\Omega_{\mathrm{PE}},\Omega_{\mathrm{EB}}) = \frac{1}{2\pi}\int_0^{2\pi}\sum_{m'=-2}^{2}\sum_{m=-2}^{2} D^{(2)}_{m,m'}(\Omega_{\mathrm{EB}})\left(D^{(2)}_{0,m}(\Omega_{\mathrm{PE}}) - \frac{\eta_\lambda}{\sqrt{6}}\left(D^{(2)}_{-2,m}(\Omega_{\mathrm{PE}}) + D^{(2)}_{2,m}(\Omega_{\mathrm{PE}})\right)\right)d\gamma_{\mathrm{EB}}$$
$$= \sum_{m=-2}^{2} D^{(2)}_{m,0}(\Omega_{\mathrm{EB}})\left(D^{(2)}_{0,m}(\Omega_{\mathrm{PE}}) - \frac{\eta_\lambda}{\sqrt{6}}\left(D^{(2)}_{-2,m}(\Omega_{\mathrm{PE}}) + D^{(2)}_{2,m}(\Omega_{\mathrm{PE}})\right)\right). \quad \text{(S2)}$$

Here, $D^{(2)}_{m',m}(\Omega_{\mathrm{XY}})$ (with $\Omega_{\mathrm{XY}} = (\alpha_{\mathrm{XY}}, \beta_{\mathrm{XY}}, \gamma_{\mathrm{XY}})$) denotes the *m',m* element of a second-rank Wigner rotation matrix (see definitions in Ref. (S5)).

The resonance frequency for a particular orientation of the bilayer (Ω_{BL}) is given by

$$\nu_\lambda(\Omega_{\mathrm{BL}}) = S_\lambda(PS)\left(\lambda_{\mathrm{iso}} + \lambda^{\mathrm{reduced}}_{\mathrm{aniso}} D^{(2)}_{0,0}(\Omega_{\mathrm{BL}})\right), \quad \text{(S3)}$$

where $S_\lambda(PS)$ is a pulse-sequence (*PS*) dependent scaling factor for the given interaction. In the present work we consider the continuous wave (CW), FSLG, and SLF (PISEMA) pulse sequences with the following theoretical scaling factors: S_b(CW) = 0, S_δ(CW) = 1; S_b(FSLG) = $\pm 1/\sqrt{3}$, S_δ(FSLG) = 1; S_b(SLF) = $\pm\sqrt{2/3}$, S_δ(SLF) = 0, where the SLF scaling factors refer to the indirect (dipolar) dimension.

The orientational disorder of the bilayer (e.g., from mosaic spread) is accounted for by a static Gaussian distribution of β_{BL} with the half width at half height $\Delta\beta_{\mathrm{BL}}$ of the bilayer normal relative to the laboratory frame (S13-16). The spectrum is calculated by a "powder" average of the orientational disorder using Eq. (S3). The spectral intensity, $I(\beta_{\mathrm{BL}})$, corresponding to the particular orientation is given by the Gaussian distribution

$$I(\beta_{\mathrm{BL}}) = \frac{1}{W}\exp\left\{-\ln 2\left(\frac{\beta_{\mathrm{BL}}}{\Delta\beta}\right)^2\right\}\sin(\beta_{\mathrm{BL}}). \quad \text{(S4)}$$

W is a scaling factor ensuring that the total intensity is 1, and the factor $\sin(\beta_{\mathrm{BL}})$ originates from the spherical integration and has the inconvenience that the intensity is zero for $\beta_{\mathrm{BL}} = 0$ if we choose a set of β_{BL}-angles with equidistant spacing. However, if we choose β_{BL} angles such that $\cos(\beta_{\mathrm{BL}})$ has equidistant spacing, the sinus term drops out of Eq. (S4). The β_{BL}-values range from $0 \le \beta_{\mathrm{BL}} \le \beta_{\max}$, where the upper value $\beta_{\max} = 4\Delta\beta_{\mathrm{BL}}$ corresponding to $I(\beta_{\mathrm{BL}}) \approx 10^{-5}$ (disregarding the sinus term). To ensure convergence of the "powder" averaging, the number of angles, *n*, corresponds to approximately one angle per degree, but with the $\cos(\beta_{\mathrm{BL}})$-distribution, the angle set (for $\beta_{\max} < 90°$) is given by

$$\beta_{\mathrm{BL}}(i) = \cos^{-1}\left(1 - \frac{i}{n}\left(1 - \cos(\beta_{\max})\right)\right)$$
$$I(\beta_{\mathrm{BL}}(i)) = \frac{1}{W}\exp\left\{-\ln 2\left(\frac{\beta_{\mathrm{BL}}(i)}{\Delta\beta}\right)^2\right\}, \qquad \text{(S5)}$$

for i-values ranging from 0 to n-1. The normalization factor, W, is given by $W = \sum_{i=0}^{n-1} I(\beta_{\mathrm{BL}}(i))$.

In practical terms, we have used SIMMOL to calculate the reduced anisotropies ($\lambda_{\mathrm{aniso}}^{\mathrm{reduced}}$) using Eqs. (S1) and (S2), and used these values as input to SIMPSON files calculating the spectrum for a given pulse sequence, where the mosaic spread is included as a "powder" averaging as described above.

4. Comparison between experimental and simulated spectra

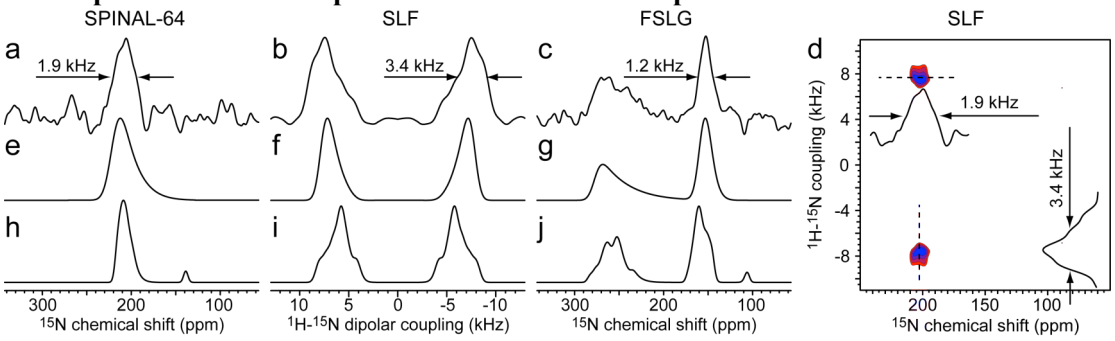

Figure S1. (a-d) Experimental and (e-j) simulated 16.45-T ^{1}H-^{15}N spectra for a sample of ^{15}N-Aib$_8$ alamethicin in oriented lipid bilayers. The spectra are obtained using (a,e,h) heteronuclear SPINAL-64 ^{1}H decoupling and (c,g,j) ^{1}H homonuclear FSLG decoupling. (d) Two-dimensional SLF (PISEMA) experiment and (b,f,i) traces along the indirect dimension at approximately 200 ppm. (e-g) Simulations assuming a single molecular conformation (corresponding to an α-helix conformation of τ,ρ = 7.85°, 52°) and Δβ = 18° for the mosaic spread. (h-j) Simulations obtained using the average chemical-shift and dipole-dipole coupling frequencies for the 25 molecules in the MD simulation. See Section 5 for details.

Fig. S1 shows the experimental 1D ^{15}N spectra recorded using heteronuclear and homonuclear decoupling as well as a 2D SLF experiment. The simulations in Fig. S1e-g represent simulations which assume a single peptide conformation in the bilayer but with a quite large value for the mosaic spread. The lower panel (Fig. S1h-j) represents simulations based on average molecular conformations from the MD simulation. Overall we observe a good agreement between the simulations and experimental data. Especially, we note that the accurate reproduction of the differential linebroadening in the simulations support our two models for the spectrum interpretation.

We note that in particular the FSLG simulation using a single molecular conformation (Fig. S1f) is illustrative for the differential linebroadening. Here, we clearly observe the narrow downfield peak with a net anisotropy close to zero and a broad upfield peak with a

large net anisotropy because the effective ^{15}N chemical shift anisotropy and ^{1}H-^{15}N dipole-dipole coupling cancel and add to each other, respectively for the two peaks.

5. Coarse-grained MD simulation

An all-atom (AA) system setup consisting of alamethicin, DMPC lipids, and water was equilibrated and converted to a coarse-grained (CG) representation, and 1 μs of CG MD simulation was carried out.

The system was built with a peptide:lipid ratio of 1:13.2 using 25 peptides and 330 lipids. Monomer C of the X-ray structure (pdb-code: 1AMT) of alamethicin (S17) was used as the initial alamethicin model. The peptide helices were placed strictly parallel to the membrane normal aligned along the *z*-axis and only translated in the *xy* plane to form a five by five lattice, with the peptide center of mass (CM) separated in the *x* and *y* directions by 28.5 Å. With the peptides in place, a DMPC lipid was replicated, rotated around its *z*-axis in a random manner, and translated to fill out the space between the peptides and form the bilayer. The lipid bilayer with peptides was then solvated in water. Alamethicin has only one potentially charged residue, namely Glu_{18}. However, we keep Glu_{18} protonated in the simulations and therefore no counter-ions are added. The initial AA setup was energy-minimized and equilibrated (200 ps) with peptides fixed. The peptides were then released followed by another energy-minimization and equilibration (1 ns). The equilibration was done in the NPT ensemble (T = 323 K, p = 1 atm.) using NAMD (S18) and the CHARMM27 parameter set (S19).

The peptide-lipid system was transferred to a CG representation and hydrated, giving a CG setup with 11,773 beads and a box size of 120 Å x 124 Å x 90 Å. The CG model applied in this work was developed by Marrink and co-workers (S20) for lipid-water systems and extended to proteins by Shih *et al.* (S21). Two CG beads in general represent amino acids: a backbone bead and a side-chain bead. Since alamethicin has non-standard residues, a few extensions to the model became necessary. The only difference between alanine (Ala) and Aib is the extra methyl group on C^{α} in Aib, and therefore a backbone bead and two side-chain beads identical to the Ala side-chain bead represent Aib. Since the protonated Glu_{18} can act as both a hydrogen bond donor and hydrogen bond acceptor, it has the same chemical class in the CG model as glutamine. The differences between phenylalanine (Phe) and phenylalaniol (Phl) have no effect in the CG model, and Phl is consequently represented as if it were a Phe. The N-terminal acetyl group is represented by a backbone bead. After energy minimization of the CG system, the production run of 1 μs was started. The simulations were carried out using a modified version of NAMD (S18) implementing the model of Shih *et al*. (S21). The temperature was kept at 323 K using a Langevin thermostat with a damping coefficient of 0.5 ps^{-1}. The pressure was kept at 1 atm using Periodic Boundary Conditions (PBC) and a Nosé-Hoover Langevin piston (S22) with a piston period of 200 fs and a decay time of 100 fs.

Nonbonded interactions were cut off at 12 Å, with shifting throughout the interaction range for electrostatic interactions and beginning at 9 Å for van der Waals interactions to implement a smooth cutoff. Pair lists were updated at least once per 20 steps, with a 16 Å pair list cutoff. The simulations were performed using a 20 fs time step.

The helix tilt angle (τ) of a peptide at a given time was found as the angle between the *z*-axis (the membrane normal) and the "helix axis" going from the CM of the backbone beads of residues 1, 2, 3, and 4 to the CM of the backbone beads of residue 10, 11, 12, and 13. The plane spanned by the "helix axis" and the *z* axis defined the zero-point for the rotational pitch angle (ρ), which was defined as the angle between this plane and an axis going perpendicularly from the "helix axis" through the CM of the two side-chain beads of Aib_8. We have verified that this definition agrees with our normal definition (based on the C^{α} position) (S2) within ~1° for the rotational pitch, assuming that the Aib side-chain beads are located approximately at the position of the C^{β} atoms.

The time-averaged tilt angles reported in Figure 1 were achieved by calculating the effective amide ^{1}H-^{15}N dipole-dipole coupling and ^{15}N chemical shift for Aib_8 at each time frame and then back-calculate the tilt angle and rotational pitch from the time average of these nuclear spin interactions. To avoid problems from the initial equilibration, the first 200 ns were excluded from this calculation, and the averages include 2000 time frames in 0.4 ns steps from 200 ns to 1 μs.

References

(S1) Ogrel, A.; Shvets, V. I.; Kaptein, B.; Broxterman, Q. B.; Raap, J. *Eur. J. Org. Chem.* 2000, 857.
(S2) Bertelsen, K.; Pedersen, J. M.; Rasmussen, B. S.; Skrydstrup, T.; Nielsen, N. C.; Vosegaard, T. *J. Am. Chem. Soc.* 2007, *129*, 14717.
(S3) Sinha, N.; Grant, C. V.; Wu, C. H.; De Angelis, A. A.; Howell, S. C.; Opella, S. J. *J. Magn. Reson.* 2005, *177*, 197.
(S4) Wu, C. H.; Ramamoorthy, A.; Opella, S. J. *J. Magn. Reson. A* 1994, *109*, 270.
(S5) Bak, M.; Rasmussen, J. T.; Nielsen, N. C. *J. Magn. Reson.* 2000, *147*, 296.
(S6) Vosegaard, T.; Malmendal, A.; Nielsen, N. C. *Chem. Monthly* 2002, *133*, 1555.
(S7) Bak, M.; Schultz, R.; Vosegaard, T.; Nielsen, N. C. *J. Magn. Reson.* 2002, *154*, 28.
(S8) Cady, S. D.; Goodman, C.; Tatko, C. D.; DeGrado, W. F.; Hong, M. *J. Am. Chem. Soc.* 2007, *129*, 5719.
(S9) Prongidi-Fix, L.; Bertani, P.; Bechinger, B. *J. Am. Chem. Soc*. 2007, *129*, 8430.
(S10) Wu, C. H.; Ramamoorthy, A.; Gierasch, L. M.; Opella, S. J. *J. Am. Chem. Soc.* 1995, *117*, 6148.
(S11) Vosegaard, T.; Nielsen, N. C. *J. Biomol. NMR* 2002, *22*, 225.
(S12) Vosegaard, T.; Kamihira-Ishijima, M.; Watts, A.; Nielsen, N. C. *Biophys. J.* 2008, *94*, 241.
(S13) Nevzorov, A. A.; Moltke, S.; Heyn, M. P.; Brown, M. F. *J. Am. Chem. Soc.* 1999, *121*, 7636.
(S14) Bechinger, B.; Sizun, C. *Concepts Magn. Reson.* 2003, *18A*, 130.
(S15) Aisenbrey, C.; Bechinger, B. *Biochemistry* 2004, *43*, 10502.
(S16) Lopez, J. J.; Mason, A. J.; Kaiser, C.; Glaubitz, C. *J Biomol NMR* 2007, *37*, 97.
(S17) Fox, R. O., Jr.; Richards, F. M. *Nature* 1982, *300*, 325.

(S18) Phillips, J. C.; Braun, R.; Wang, W.; Gumbart, J.; Tajkhorshid, E.; Villa, E.; Chipot, C.; Skeel, R. D.; Kale, L.; Schulten, K. *J. Comput. Chem.* 2005, *26*, 1781.
(S19) MacKerell, A. D.; Bashford, D.; Bellott, M.; Dunbrack, R. L.; Evanseck, J. D.; Field, M. J.; Fischer, S.; Gao, J.; Guo, H.; Ha, S.; Joseph-McCarthy, D.; Kuchnir, L.; Kuczera, K.; Lau, F. T. K.; Mattos, C.; Michnick, S.; Ngo, T.; Nguyen, D. T.; Prodhom, B.; Reiher, W. E.; Roux, B.; Schlenkrich, M.; Smith, J. C.; Stote, R.; Straub, J.; Watanabe, M.; Wiorkiewicz-Kuczera, J.; Yin, D.; Karplus, M. *J. Phys. Chem. B* 1998, *102*, 3586.
(S20) Marrink, S. J.; de Vries, A. H.; Mark, A. E. *J. Phys. Chem. B* 2004, *108*, 750.
(S21) Shih, A. Y.; Arkhipov, A.; Freddolino, P. L.; Schulten, K. *J. Phys. Chem. B* 2006, *110*, 3674.
(S22) Scott, E. F.; Yuhong, Z.; Richard, W. P.; Bernard, R. B. *J Chem Phys* 1995, *103*, 4613.